CA1i pyramidal neurons mediate the role of NMDA receptor subunit GluN3A in depressive behavior and D-serine anti-depression

Wei Zhang[1,2]†, Jiesi Wang[1]†*, Jiajie Dai[1,2], Linan Zhuo[1,2], Mingyue Zhao[1,2], Haimou Ye[1,2], Weiwen Wang[1,2*]

[1]Key Laboratory of Mental Health, Institute of Psychology, Chinese Academy of Sciences, Beijing, 100101, China

[2]Department of Psychology, University of Chinese Academy of Sciences, Beijing, China

†These authors contributed equally to this work

*Correspondence:

Weiwen Wang, Key Laboratory of Mental Health, Institute of Psychology, No. 16 Lincui Road, Chaoyang District, Beijing, 100101, China.

Email: wangww@psych.ac.cn

Jiesi Wang, Key Laboratory of Mental Health, Institute of Psychology, No. 16 Lincui Road, Chaoyang District, Beijing, 100101, China.

Email: wangjs@psych.ac.cn

Abstract

Depression is a heterogeneous psychiatric disorder characterized by multiple symptom clusters. N-methyl-d-aspartic acid receptors (NMDARs), consisting of various subunit proteins GluN1-3, are known to be critical molecular bases for the occurrence and treatment of depression. However, the involvement of the NMDAR subunit GluN3A in the heterogeneity of depressive symptoms and antidepressant effects remains unclear. Here, we found that chronic social defeat stress (CSDS) induced a range of depression-related behaviors, including decreased social interest, increased helplessness and anxiety-like behavior, and reduced GluN3A mRNA and protein expression in the hippocampal CA1 intermediate (CA1i) region. Additionally, GluN3A knockout (KO) mice exhibited pronounced helplessness behavior. Increasing GluN3A expression in the CA1i in both models specifically reversed the increased helplessness behavior but not social interest and anxiety-like behavior. Furthermore, the lack of CA1i GluN3A expression reduced the activity of CA1i pyramidal neurons in mice during helplessness behavior, a phenomenon also reversed by upregulating CA1i GluN3A expression. Further bidirectional modulation of CA1i pyramidal neuron activity directly mimicked or reversed CSDS-induced helplessness behavior. Finally, injection of D-serine into the CA1i rapidly improved helplessness behavior in CSDS mice while increasing the activity of CA1i pyramidal neurons, whereas knockout of the GluN3A or inhibition of CA1i neuron activity prevented the effect of D-serine. Our study elucidates the critical role of GluN3A subunit in regulating depression-related helplessness behavior and its mechanisms, as well as its role in the

rapid antidepressant effect of D-serine, which deepen the understanding of the complex pathophysiology of depression and develop a potential clinical treatment new target.

Keywords: Depression-related behavior, NMDA receptor, GluN3A subunit, Hippocampus, Pyramidal neurons, D-serine

Introduction

Depression is one of the most prevalent psychiatric disorders worldwide, affecting over 350 million people globally and standing as a leading cause of disability and a significant economic burden[1, 2]. Meanwhile, current clinical treatments, which primarily target the monoaminergic system, are challenged by limited and delayed efficacy, as well as adverse effects [3-6]. Currently, depression is increasingly recognized as a complex clinical syndrome manifested by a heterogeneous disease consisting of a set of symptomatic clusters in emotion, cognition and others [7-10]. A growing body of clinical and basic evidence has shown that there are specific pathological mechanisms underlying various symptoms or sub-types of depression[7, 11-13]. Therefore, to address these challenges, it is crucial to elucidate the complex psychopathological mechanisms underlying the heterogeneous symptoms and develop more effective and targeted treatment strategy for depression.

The N-methyl-D-aspartate receptor (NMDAR), an ionotropic glutamate receptor, plays a pivotal role in depression[14-17]. It has been shown that adaptive changes in NMDAR subunits accompany with chronic efficacy of clinical antidepressant drugs like imipramine and citalopram[15, 18-20]. NMDAR antagonists, such as ketamine, exert rapid and lasting antidepressant effects by restoring neuroplasticity of emotion-related brain regions, such as hippocampus and prefrontal cortex[21-26]. NMDARs consist of heterotetrametric structures, with two obligatory GluN1 subunits and the remaining subunits composed of GluN2 (GluN2A/B/C/D) or GluN3 (GluN3A/B) in various combination[27, 28]. Studies have shown that different subunit compositions

of NMDARs result in distinct ion channel and ligand-binding properties, thereby differentially regulating the structure and function of brain regions[29-32]. The GluN3A subunit, the most expressed GluN3 subunit, is currently considered as a molecular "balancer" of NMDAR due to its unique ion channel properties, including low calcium permeability, low sensitivity to Mg^{2+} block, and a lower and longer channel opening time[31-35]. Several studies have reported that the GluN3A can modulate synaptic plasticity by altering NMDAR-mediated currents and neuronal long-term potentiation (LTP) responses[36-39]. Specifically, GluN3A has been found to be highly expressed in cognition and emotion related brain regions, such as the prefrontal cortex, hippocampus and amygdala[28, 32, 40], and is involved in brain maturation processes and emotion regulation, such as fear and aversion behavior[34, 40-43]. Several clinical studies have also reported that the polymorphism of *GRIN3A* gene may be related with the increased risk of psychiatric disorders, including bipolar disorder and schizophrenia[35, 44]. However, the roles of the GluN3A in depression-related behaviors remain unclear.

The structural and functional abnormalities of hippocampus have been recognized as important pathophysiological bases in depression and targets involved in the efficacy of antidepressant therapy[45-47]. Extensive alterations in the number and morphology of neurons and synapses, as well as LTP and long-term depression (LTD) response in hippocampus are reported in depressive patients and animal models[48-50]. The restoration of hippocampal abnormalities is consistent with the amelioration of depressive symptoms after chronic antidepressant treatment[15].

However, the hippocampus is a complex structure with multiple subregions, such as CA1, CA2/3, and dentate gyrus (DG)[51]. The recent researches with spatial transcriptome technology further discriminated the finer spatial-specific functional heterogeneity of hippocampus[52, 53]. For example, the dorsal, intermediate, and ventral regions of subregions like CA1, CA3, and DG exhibit distinct molecular expression and neural projection circuit characteristics[53, 54]. Notably, one study also identified a spatial distribution characteristic of GluN3A in the hippocampus, with a more centralized expression in the intermediate and ventral pyramidal cell layers of CA1[53]. Therefore, it is important to focus on the relationship between GluN3A subunit in different hippocampal subregions and the heterogeneous symptoms of depression.

Noteworthy, the NMDAR subunits GluN3 and GluN1 have unique ligand-binding characteristics due to their presence of the glycine-binding (GB) site, which can bind to endogenous agonists glycine and D-serine, but not glutamate, which binding to GluN2 subunits[33, 40, 55, 56]. The GB site has been an important target for antidepressant development, and several chemical compounds binding to this site, such as cycloserine, GLYX-13, as well as D-serine, have shown rapid antidepressant effects or enhanced the effects of current antidepressant treatments in preclinical studies and clinical trials[57-61]. For example, several animal studies have demonstrated that D-serine can exert rapid antidepressant effects, and hippocampus is an important area for its efficacy[61-63]. Additionally, considering the stronger affinity of GluN3A for the ligand D-serine compared to the GluN1 subunits, its role in

the antidepressant effects of D-serine may provide an insight into the molecular mechanisms of rapid antidepressant[64].

Therefore, based on the chronic social defeat stress (CSDS) induced animal model of depression and GluN3A knockout mice, combining comprehensive approaches encompassing behavior, molecular biology, genetic regulation, microscopic imaging, fiber recording, and pharmacology, we systematically investigated the role of hippocampal GluN3A in depression and in the antidepressant effect of D-serine.

Experimental design

This research is divided into the following sections:

Section 1. Utilizing the classical CSDS model and GluN3A KO animals, we systematically investigated the behavioral manifestations of various depression phenotypes in these animal models, as well as the changes in mRNA and protein expression of GluN3A in several emotion-related brain regions, especially in various subregions of the hippocampus, including CA1 dorsal (CA1d), CA1i, CA1 ventral (CA1v), CA3 and DG. This was done to identify the potentially functional brain region (target brain region) where GluN3A may regulate depression-related behaviors.

Section 2. Based on the findings from Section 1, we investigated the effect of CA1i microinjection of GluN3A overexpression adeno-associated virus (AAV) on the depression-related behavior in CSDS model and GluN3A KO model animals. The aim was to confirm whether the CA1i region plays a critical role in the modulation of depression-related behavior by the GluN3A subunit.

Section 3. Based on the previous sections, immunofluorescence staining and fiber photometry were used to detect neuronal functional activities in the CA1i region of CSDS model and GluN3A KO model animals during the helplessness test. Subsequently, chemogenetic approaches were used to modulate the functional activities of CA1i neurons during the helplessness behavior in CSDS mice and normal mice. The aim of these investigations was to identify the neuronal bases of CA1i GluN3A in regulating helplessness behavior.

Section 4. This section aimed to investigate whether the antidepressant effect of D-serine is mediated by the GluN3A subunit and activation of CA1i pyramidal neurons. This was achieved by microinjection of D-serine into CA1i in CSDS mice GluN3A KO mice, as well as the CA1i neuronal activity inhibited mice, to compare the behaviors with corresponding controls. Furthermore, immunofluorescence staining was utilized to examine the impact of these interventions on the number of c-Fos-positive cells in the pyramidal neurons of CA1i.

Results

Effects of CSDS and GluN3A KO on depression-related behaviors and GluN3A expression in hippocampus

We systematically evaluated various depression-related behaviors induced by CSDS in mice (Fig. 1a, b). Regarding the anhedonia indicator, CSDS mice showed a significant reduction in social interaction ratio ($t_{16} = 5.802$, $^{***}P < 0.001$, Fig. 1c, d) in the social interaction test (SIT) but no significant change in sucrose preference ratio ($P > 0.05$, Supplementary Fig. 1a) in the sucrose preference test (SPT) compared to

the control group. In terms of helplessness behavior, CSDS significantly increased the immobile time of mice in the tail suspension test (TST) (t_{14} = 2.877, $^{*}P$ = 0.012, Fig. 1e) and forced swim test (FST) (t_{11} = 2.240, $^{*}P$ = 0.047, Fig. 1f). In locomotor activity, compared to the control group, CSDS did not affect the total distance traveled by mice ($P > 0.05$, Fig. 1g, h). Regarding anxiety-related indicators, CSDS markedly induced anxiety-like behavior in mice, evidenced by decrease in the number of entries of centre area (t_{11} = 2.069, P = 0.063, Fig. 1i) and the time spent in the centre area (Welch-corrected $t_{6.666}$ = 2.625, $^{*}P$ = 0.036) in the open field test (OFT) (Fig. 1g, j). Additionally, in the elevated plus maze (EPM), CSDS mice exhibited a reduction in the number of the open arm entries (Welch-corrected $t_{11.43}$ = 2.232, $^{*}P$ = 0.047, Fig. 1k, l) and the open arm time ratio (Welch-corrected $t_{8.989}$ = 2.206, P = 0.055, Fig. 1k, m). These results indicated that CSDS successfully induced various depressive phenotypes in mice.

Subsequently, we examined the changes in GluN3A expression levels in various emotion-related brain regions, particularly the hippocampus, in mice following CSDS (Supplementary Fig. 1c). The quantitative real-time PCR (qRT-PCR) results showed a significant reduction in GluN3A expression in the CA1i region of the hippocampus in CSDS mice compared to the control group (t_{23} = 2.692, $^{*}P$ = 0.013, Fig. 1n), while there were no significant changes in the other subregions of the hippocampus, including CA1d, CA1v, CA3, and DG ($P > 0.05$, Fig. 1n). Furthermore, in the medial prefrontal cortex (mPFC) and basolateral amygdala (BLA) of CSDS mice, the GluN3A mRNA expression was not significant changed compared to the control

group ($P > 0.05$, Supplementary Fig. 1d). The western blot results similarly demonstrated a significant decrease of GluN3A protein expression in the CA1i in CSDS mice ($t_9 = 2.866$, $^*P = 0.024$), with no significant changes observed in CA1v and CA3 ($P > 0.05$, Fig. 1o, p). These data indicated a downregulation of GluN3A expression in the hippocampal CA1i region of by CSDS in mice.

To further examine the relationship between GluN3A and depression-like behaviors, we conducted behavioral tests on GluN3A KO mice under physiological conditions (Fig. 1q). On the anhedonia indicators, GluN3A KO mice did not exhibit an abnormal ratio of social interactions ($P > 0.05$, Fig. 1r) and sucrose preference ($P > 0.05$, Supplementary Fig. 2a) compared to wild-type (WT) mice. In contrast, the results showed that GluN3A KO mice exhibited a phenotype of helplessness compared to WT mice, as evidenced by significant increased immobile time in TST ($t_{16} = 2.778$, $^*P = 0.013$, Fig. 1s) and FST ($t_{14} = 2.457$, $^*P = 0.028$, Fig. 1t). In addition, GluN3A KO did not influence the locomotor activity ($P > 0.05$, Fig. 1u) and anxiety-like behavior ($P > 0.05$, Fig. 1v-y).

To ascertain whether GluN3A KO is associated with an increased susceptibility to social defeat stress (SDS), a systematic assessment was conducted to evaluate the effects of subthreshold SDS on depression-related behaviors in GluN3A KO mice. The results showed GluN3A KO mice subjected to subthreshold SDS exhibited a similar significant increase in immobile time in the FST (Welch-corrected $t_{2.520} = 9.677$, $^*P = 0.031$, Supplementary Fig. 2d), but no significant changes observed in social interest, sucrose preference, locomotor activity, and anxiety-like behavior ($P >$

0.05, Supplementary Fig. 2b, c, e, g-i), with the exception of a significant reduction in the number of entries of centre area in the OFT (t_{13} = 2.815, $^{*}P$ = 0.015, Supplementary Fig. 2f). The data indicated that the GluN3A KO does not influence the susceptibility of mice to SDS.

Taken together, these results suggested that the decreased expression of GluN3A in the brain was involved in the manifestation of depression-related behaviors, and that the hippocampal CA1i may be a potential brain region for the regulation of depression-related behaviors by GluN3A.

Rescue of the GluN3A decline in CA1i neurons reversed helplessness behaviors

We further investigated the regulatory role of CA1i GluN3A in depression-related behaviors, by using AAV to upregulate GluN3A expression in the CA1i of CSDS mice (Fig. 2a, b). We found that the upregulation of GluN3A did not affect the anhedonia behaviors of CSDS mice. Specifically, two-way ANOVA for SIT showed a significant main effect of stress (i.e., control or stress) ($F_{(1, 25)}$ = 8.488, $^{**}P$ = 0.007, Fig. 2c), with post-hoc analysis revealing a borderline decrease in social interaction ratio in the stress:AAV-ZsGreen group compared to the control:AAV-ZsGreen group (FDR-corrected P = 0.064). There were no significant effects observed in SPT ($P >$ 0.05, Supplementary Fig. 3a). The upregulation of GluN3A subunit reversed the helplessness behavior induced by CSDS. Specifically, two-way ANOVA for TST showed a significant interaction effect ($F_{(1, 28)}$ = 5.568, $^{*}P$ = 0.026, Fig. 2d), with post-hoc analysis revealing a significant increase in immobile time in the stress:AAV-

ZsGreen group compared to the control:AAV-ZsGreen group (FDR-corrected $^{*}P$ = 0.024), while the stress:AAV-Grin3A group showed a significant decrease in immobile time compared to the stress:AAV-ZsGreen group (FDR-corrected $^{*}P$ = 0.016). Two-way ANOVA for FST showed significant main effects of stress ($F_{(1, 28)}$ = 5.010, $^{*}P$ = 0.033, Fig. 2e) and viral treatment (i.e., AAV-ZsGreen or AAV-Grin3A) ($F_{(1, 28)}$ = 12.99, $^{**}P$ = 0.0012) on the immobile time, with post-hoc analysis showing a significant increase in immobile time in the stress:AAV-ZsGreen group compared to the control:AAV-ZsGreen group (FDR-corrected $^{*}P$ = 0.026) and a significant decrease in immobile time in both the control:AAV-Grin3A group (FDR-corrected $^{*}P$ = 0.036) and stress:AAV-Grin3A group (FDR-corrected $^{*}P$ = 0.016) compared to their respective AAV-ZsGreen groups. Furthermore, the upregulation of GluN3A subunit did not affect the locomotor activity and the anxiety-like behavior. Specifically, two-way ANOVA revealed a significant main effect of stress on the total distance traveled ($F_{(1, 29)}$ = 13.88, $^{***}P < 0.001$, Fig. 2f), with post-hoc analysis showing a significant decrease in total distance traveled in the stress:AAV-ZsGreen group (FDR-corrected $^{*}P$ = 0.024) and stress:AAV-Grin3A group (FDR-corrected $^{*}P$ = 0.016) compared to the control:AAV-ZsGreen group and control:AAV-Grin3A group, respectively. Consistent with the previous experiments, CSDS induced the increase of multiple anxious indicators in OFT and EPM (Fig. 2g-j), but which were not affected by the upregulation of GluN3A subunit. These results indicated that the CA1i GluN3A modulated CSDS-induced helplessness behaviors in mice.

To further investigate the direct regulatory relationship between the CA1i

GluN3A and helplessness behaviors, we restored the GluN3A in the CA1i region of GluN3A KO mice using AAV (Fig. 2k). Similarly, the results showed that the restoration of GluN3A reversed of the indicators of helplessness behavior (Fig. 2l, m). However, there were no significant changes observed in social interest, locomotor activity, and anxiety-like behavior ($P > 0.05$, Fig. 2n and Supplementary Fig. 3b-d). Specifically, GluN3A KO mice showed a significant increase in immobile time in TST ($t_{12} = 2.212$, $^{*}P = 0.047$, Fig. 2l) and FST ($t_{11} = 2.309$, $^{*}P = 0.041$, Fig. 2m) compared to WT mice, while GluN3A KO:AAV-Grin3A mice exhibited a significant restoration of immobile time to normal levels in both TST ($t_{10} = 2.696$, $^{*}P = 0.023$) and FST ($t_{10} = 2.912$, $^{*}P = 0.016$) compared to GluN3A KO mice. In summary, hippocampal CA1i GluN3A played a crucial role in regulating depression-related helplessness behavior.

Activity of pyramidal neurons in CA1i mediated the regulation of GluN3A in helplessness behavior

After upregulating GluN3A subunit expression in CSDS mice, we further investigated the functional activity of CA1i neurons during helplessness behavior. The results of c-fos immunostaining showed that there was decreased functional neuronal activity in the CA1i pyramidal layer after the FST in stressed mice compared with the controls (Fig. 3a-c), which was restored by upregulating GluN3A. Specifically, two-way ANOVA analysis of the number of c-Fos-positive cells showed significant interaction ($F_{(1, 20)} = 4.820$, $^{*}P = 0.040$, Fig. 3b) and stress main effects ($F_{(1, 20)} = 6.015$, $^{*}P = 0.024$), with a marginal significant effect for viral treatment ($F_{(1, 20)} =$

3.679, P = 0.070). Post-hoc analysis revealed a significant decrease in the number of c-Fos-positive cells in the stress:AAV-ZsGreen group compared to the control:AAV-ZsGreen group (FDR-corrected $^{**}P$ = 0.009), while the stress:AAV-Grin3A group showed a significant increase in the number of c-Fos-positive cells compared to the stress:AAV-ZsGreen group (FDR-corrected $^{**}P$ = 0.009).

Furthermore, we examined the direct relationship between GluN3A subunit and neuronal functional activity in the CA1i pyramidal layer after the FST in GluN3A KO mice. Immunostaining results showed that the number of c-Fos-positive cells were significantly increased after FST compared with basal condition (no FST experience) in WT mice (t_9 = 2.884, $^{*}P$ = 0.018), and such activation did not occur in FST-experienced GluN3A KO mice (t_{10} = 3.232, $^{**}P$ = 0.009, Fig. 3d, e), indicating that the activation of neurons in the CA1i pyramidal layer involved in FST behavior, while the absence of GluN3A resulted in this kind of functional defect.

Moreover, we validated the necessity of GluN3A in the activation of excitatory neurons in the CA1i pyramidal layer during the TST using fiber photometry (Fig. 3f). During TST, GCaMP signal characterizing excitatory neurons calcium levels correlated with the active state of the mice, and the rise of signal was behind the transition from immobile state to struggling state (Fig. 3g). Subsequently, we observed that the average peak amplitude of neuronal responses significantly increased during events when mice transitioned from immobility to struggling (Fig. 3h, i), with WT mice showing significantly higher neuronal activation responses during the struggling phase compared to GluN3A KO mice (t_9 = 3.398, $^{**}P$ = 0.008,

Fig. 3j).

Collectively, these results indicated that the activation of CA1i pyramidal neurons mediated the regulation of GluN3A subunit in helplessness behavior in mice.

Bidirectional chemogenetic modulation of CA1i pyramidal neurons directly mimicked or reversed the CSDS-induced helplessness behavior

Next, we investigated the direct role of CA1i pyramidal neuronal activity in depression-related helplessness behavior. We first increased the activity of CA1i pyramidal neurons using AAV-hM3D(Gq) in combination with different concentrations of clozapine-N-oxide (CNO) (Fig. 4a). The results showed that saline, 0.05 mg/kg, 0.2 mg/kg, and 0.5 mg/kg CNO did not affect the locomotor activity and anxiety-like behavior of normal mice in the OFT and rotarod test (RT) ($P > 0.05$, Supplementary Fig. 4a-d). However, one-way ANOVA showed that concentrations of 0.2 mg/kg (FDR-corrected $^{**}P = 0.009$, Fig. 4b-c, Supplementary Fig. 4e) and 0.5 mg/kg (FDR-corrected $^{**}P = 0.009$) CNO effectively increased the number of c-Fos-positive cells at the injection site ($F_{(2, 3)} = 16.89$, $^{*}P = 0.023$). Therefore, we chose a concentration of 0.2 mg/kg CNO for subsequent chemogenetic activation experiments (Fig. 4d). The results indicated that the activation of CA1i pyramidal neuronal activity in CSDS mice partially enhanced social interest in the SIT (Fig. 4e), and reversed the helplessness behavior induced by CSDS in the TST and FST (Fig. 4f, g), but did not alter their locomotor activity and anxiety-like behavior in the OFT (Fig. 4h-j). Specifically, two-way ANOVA for the social interaction ratio showed a significant viral treatment main effect ($F_{(1, 20)} = 6.983$, $^{*}P = 0.016$, Fig. 4e). Two-way ANOVA

for immobile time in the TST showed a significant interaction effect ($F_{(1, 22)} = 6.923$, $^{*}P = 0.015$, Fig. 4f), with post-hoc analysis showing a significant increase in immobile time in the stress:AAV-mCherry group compared to the control:AAV-mCherry group (FDR-corrected $^{*}P = 0.011$), while the stress:AAV-hM3D(Gq) group exhibited a significant decrease in immobile time to normal levels compared to the stress:AAV-mCherry group (FDR-corrected $^{*}P = 0.011$). Two-way ANOVA for immobile time in the FST showed significant stress ($F_{(1, 21)} = 5.350$, $^{*}P = 0.031$, Fig. 4g) and viral treatment main effects ($F_{(1, 21)} = 12.34$, $^{**}P = 0.002$), with post-hoc analysis showing a significant increase in immobile time in the stress:AAV-mCherry group compared to the control:AAV-mCherry group (FDR-corrected $^{*}P = 0.023$), and a significant decrease in immobile time in both the control:AAV-hM3D(Gq) group (FDR-corrected $^{*}P = 0.026$) and stress:AAV-hM3D(Gq) group (FDR-corrected $^{*}P = 0.009$) compared to their respective AAV-mCherry groups. Two-way ANOVA analysis for total distance traveled showed only a significant stress main effect ($F_{(1, 27)} = 8.267$, $^{**}P = 0.008$, Fig. 4h), with post-hoc analysis revealing a marginal decrease in total distance traveled in the stress:AAV-mCherry group compared to the control:AAV-mCherry group (FDR-corrected $P = 0.063$). These results indicated that increased the activation of neurons in CA1i can decrease CSDS-induced helplessness behavior.

On the other hand, we inhibited the activity of CA1i pyramidal neurons in normal mice using AAV-hM4D(Gi) (Fig. 4k, l). We found that reducing the activity of the neurons significantly increased immobile time in the TST ($t_{12} = 3.261$, $^{**}P = 0.007$, Fig. 4m) and FST ($t_{13} = 2.622$, $^{*}P = 0.021$, Fig. 4n), but did not induce abnormalities

in locomotor activity and anxiety-like behavior in the OFT ($P > 0.05$, Fig. 4o-q), indicating that the inhibition of neuronal activity in CA1i can directly induce phenotypes of depression-related helplessness behavior.

Overall, we demonstrated that the activity of CA1i pyramidal neurons was an underlying mechanism for the regulation of depression-related helplessness behavior by GluN3A.

Potentiation of GluN3A-mediated pyramidal neuronal activity in CA1i was crucial for the antidepressant effects of D-serine

We further explored the role of GluN3A in the rapid antidepressant effect of hippocampal D-serine administration. By injecting D-serine into the bilateral CA1i region of CSDS mice and GluN3A KO mice before behavioral testing (Fig. 5a, b), we found that D-serine could significantly reverse the helplessness behavior induced by CSDS (Fig. 5c, d), while it had no significant effect on locomotor activity and anxiety-like behavior in the OFT in all groups ($P > 0.05$, Fig. 5e-g). Specifically, two-way ANOVA for immobile time in the TST and FST showed significant interaction (Control-cerebrospinal fluid (CSF), Control-D-serine, Stress-CSF and Stress-D-serine group, TST: $F_{(1, 27)} = 6.084$, $^{*}P = 0.020$; FST: $F_{(1, 27)} = 5.106$, $^{*}P = 0.032$, Fig. 5c, d) and drug treatment main effects (TST: $F_{(1, 27)} = 11.60$, $^{**}P = 0.002$; FST: $F_{(1, 27)} = 11.19$, $^{**}P = 0.002$), with post-hoc analysis showing a significant increase in immobile time in the stress:CSF group compared to the control:CSF group in both tests (TST: FDR-corrected $^{*}P = 0.017$; FST: FDR-corrected $^{*}P = 0.032$), while the stress:D-serine group exhibited a significant decrease in immobile time compared to the stress:CSF

group (TST: FDR-corrected $^{***}P < 0.001$; FST: FDR-corrected $^{**}P = 0.002$). Interestingly, compared to the control (WT):D-serine group, the GluN3A KO:D-serine group still exhibited significant increased immobile time in both the TST ($t_{13} = 2.470$, $^{+}P = 0.028$) and FST ($t_{13} = 3.225$, $^{++}P = 0.007$), suggesting that the rapid antidepressant effect of D-serine was limited by the lack of GluN3A. Additionally, simultaneously inhibiting the activity of CA1i pyramidal neurons in CSDS mice while administering D-serine, we found that the stress-hM4D(Gi) group showed a significant increase in immobile time in both the TST ($t_{12} = 4.628$, $^{###}P < 0.001$) and FST ($t_{12} = 2.671$, $^{\#}P = 0.020$) compared to the Stress-mCherry group, indicating that the inhibition of pyramidal neuronal activity in the CA1i blocked the rapid antidepressant effect of D-serine.

Furthermore, we performed immunostaining for c-Fos in the CA1i pyramidal layer neurons of mice from the aforementioned groups after the FST (Fig. 5h). The results showed that D-serine significantly reversed the decrease in the number of c-Fos-positive cells induced by CSDS in the CA1i pyramidal layer (Fig. 5i, j). Specifically, two-way ANOVA for the number of c-Fos-positive cells showed significant stress (Control-CSF, Control-D-serine, Stress-CSF and Stress-D-serine group, $F_{(1, 16)} = 11.23$, $^{**}P = 0.004$, Fig. 5j) and drug treatment effects ($F_{(1, 16)} = 13.78$, $^{**}P = 0.002$). Post-hoc analysis showed a significant decrease in the number of c-Fos-positive cells in the stress:CSF group compared to the control:CSF group (FDR-corrected $^{*}P = 0.037$), while both the control:D-serine group (FDR-corrected $^{*}P = 0.016$) and stress:D-serine group (FDR-corrected $^{*}P = 0.045$) showed a significant

increase in the number of c-Fos-positive cells compared to their respective CSF groups. However, in GluN3A KO:D-serine mice, the number of c-Fos-positive cells in the CA1i pyramidal layer did not rise to the level of the control (WT):D-serine group (t_8 = 2.967, ^{+}P = 0.018). In summary, D-serine exerted a rapid antidepressant effect in the hippocampal CA1i region, which may depend on GluN3A-mediated activation of CA1i pyramidal neurons.

Discussion

In the present study, we systematically investigated the functions of the GluN3A subunit of the NMDAR in the regulation of depression-related behaviors. Our results demonstrated that the reduction of GluN3A expression in the hippocampal CA1i region was specifically associated with depression-related helplessness behaviors in TST and FST. Furthermore, the effects of GluN3A on helplessness may be mediated through regulating the activation of CA1i pyramidal neurons. Lastly, we found that the rapid antidepressant effect of D-serine on helplessness behavior can be reduced by GluN3A KO or inhibition of CA1i neuron activity, suggesting that GluN3A in the hippocampal CA1i pyramidal region mediated the rapid antidepressant role of D-serine. In summary, we found the GluN3A in hippocampal CA1i region plays a critical role in regulating the depression-related helplessness behaviors, which may occur through the effect of GluN3A on the activity of CA1i pyramidal neurons, and such mechanisms may also contribute the rapid antidepressant effect of D-serine.

First, we found that mice with a reduction of GluN3A in the CA1i region, either induced by CSDS or GluN3A knockout, exhibited significantly increased helplessness

behavior as measured by the FST and TST. Moreover, helplessness behavior can be reversed by selectively upregulating the expression of CA1i GluN3A, without affecting social interest and anxious behaviors. These suggest GluN3A expression in CA1i exerts direct and specific effects on helplessness in depression. In alignment with our findings, a recent study has reported that hippocampal GluN3A can influence depression-related behaviors induced by chronic restraint stress[43]. Thus, the present study further identified the specific hippocampal subregion, CA1i involved in the depression, especially helplessness behaviors. Additionally, according to the Hippocampus Gene Expression Atlas (HGEA) generated by Michael S. Bienkowski et al., the CA1 region can be further divided into four distinct subregions: CA1d, CA1i, CA1v, and ventral tip (CA1vv). Interestingly, this study also identified GluN3A as a typical marker for distinguishing between the CA1d and CA1i subdomains[53]. Thus, our results further support the validity of this more elaborated hippocampal subregion delineation in heterogeneous symptomatic cluster in depression. Helplessness or hopelessness has identified as a key symptom in depression and shown stronger associations with suicide thoughts and behavior[10, 65, 66], which was limited effected by SSRIs but can be rapidly relieved by ketamine[6, 67, 68]. In this study, targeting GluN3A, we provides a valuable animal model to elucidate the neurobiological mechanisms of helplessness phenotype.

Second, we found that CSDS mice showed reduced activity of CA1i pyramidal neurons, as represented by fewer c-Fos-positive neurons during helplessness behavior, and this was reversed by upregulating the expression of CA1i GluN3A. Consistently,

GluN3A knockout mice exhibited fewer c-Fos-positive CA1i pyramidal neurons, as well as a specific dampening of GCaMP signal of CA1i excitatory neurons during the struggle periods of the TST compared with WT mice. Additionally, we found that inhibiting CA1i pyramidal neurons activity directly increased the helplessness behavior in normal mice, while increasing their activity by chemogenetic method reversed it in CSDS mice. These results, for the first time, identified the positive regulatory effects of GluN3A on the activity of CA1i pyramidal neurons during helplessness behavior. GluN3A may act as a necessary component of NMDARs in CA1i neurons[40], thus the expression of GluN3A could directly influence the total number of membrane-bound NMDAR, which could further induce changes in Ca^{2+} influx during the behaviors, as shown by our Ca^{2+} imaging data indicating significantly reduced signal amplitude during struggling in KO animals. A previous study by Lee et al. also demonstrated that GluN3A knockout mice exhibited lower neuronal c-Fos expression and decreased phosphorylation levels of CaMKII in the olfactory bulb during olfactory discrimination tasks[69]. Li et al. also reported that activity inhibition of CA1 pyramidal neurons could facilitate the depressive behaviors induced by stress[50]. On the other hand, a recent study by Su et al. indicated that the increase CA1 neuronal activity, which induced by GluN2A inhibition, was essential for the rapid antidepressive effect of ketamine[22]. Interestingly, another recent study reported a competitive relationship between GluN3A and GluN2A at the synaptic membrane[70]. These results suggested an intrinsic mechanism of GluN3A via CA1i pyramidal neurons specifically regulating helplessness in depression.

In the final part of our study, we further explored the potential role of GluN3A in anti-depression. It is known that the GB site is localized on both the GluN1 and GluN3 subunits of the NMDAR, but the latter one showed a higher affinity for the endogenous ligand, D-serine and Glycine[33, 64]. Previous studies have reported that D-serine exerts rapid antidepressant effects in preclinical and clinical studies, and hippocampus is an import site for its antidepressant efficacy[61, 71, 72]. Thus, the current study further investigated the influence of GluN3A on the antidepressant effect of D-serine. We found that the CA1i microinjected D-serine rapidly decreased the helplessness behavior in CSDS mice but not in animals with inhibited CA1i pyramidal neurons or lack of GluN3A KO, suggesting the antidepressant effects may depend on GluN3A-mediated activation of CA1i pyramidal neurons. Given the similar effects of ketamine on the activity of hippocampal CA1 pyramidal neurons[22], our findings showed a great potential of GluN3A to be molecular target for the development of rapid-acting antidepressants.

The current study has several limitations that should be addressed in future investigations. First, we did not identify the GluN3A-expressing neuronal cell types and their specific functions in depression. A previous study by Murillo et al. has demonstrated that GluN3A in the hippocampus was localized in both pryamidal neurons and interneurons[40]. Secondly, we did not investigate the interactive effects between GluN3A and other NMDAR subunits, nor the functions of other NMDAR subunits on neuronal activity observed. Third, we did not examine the effects of GluN3A on other GB site ligands beyond D-serine.

In conclusion, our study identified the regulatory effect of the GluN3A on helplessness behavior and deciphered the underlying brain area and neuronal mechanisms. Our findings contribute to a better understanding of the heterogeneous symptom profiles in depression and related disorders, and may inform the development of more targeted and effective therapeutic strategies.

Materials and methods

Animals

All animal procedures were approved by the Institutional Animal Care and Use Committee of the Institute of Psychology, Chinese Academy of Sciences. C57BL/6N male mice and CD-1 (ICR) male mice were purchased from Charles River, Beijing, China. *Grin3A*$^{-/-}$ (GluN3A KO) mice (C57BL/6J background) were provided by Tifei Yuan's laboratory. This model was established by the construction of a specific small guide RNA (sgRNA) vector to direct Cas9 to delete exon 2 of the GluN3A gene. The GluN3A KO and WT littermates used in this study were bred from the corresponding homozygous GluN3A KO and WT mice, respectively, in the individually ventilated cage (IVC). All mice were housed in a specific-pathogen-free (SPF) environment with a temperature of 22±2℃, relative humidity of 40-70%, and a 12-hour (h) light-dark cycle (7:00 am-19:00 pm). The experimental mice had free access to food and water throughout the experimental period.

CSDS Model of Depression

CSDS was performed as previously described[11]. Male CD1 mice, singly

housed for 10-24 weeks, were screened based on aggression intensity. CD1 mice displaying attacks toward unfamiliar "intruders" within 3 minutes (min) for 3 consecutive days were designated as "residents" for subsequent stress experiments. 3 days before the CSDS experiment, "resident" CD1 mice were placed into the CSDS cage to establish territorial awareness. During each day of the 10-day CSDS period, adult C57BL/6N mice were introduced into the "resident" CD1 mouse home cage and subjected to physical attacks for 10 min. For the remainder of the day, a transparent perforated PVC divider was used to separate them while maintaining visual, auditory, and olfactory contact. For 10 successive days, a C57BL/6N mouse was introduced to a novel aggressive CD1 mouse home cage every day. C57BL/6N control mice were housed in the CSDS cage with a divider to avoid body contact, and a new cage mate was introduced every 24 hours (h) for 10 days. After the social defeat stress, the experimental mice were individually housed until all tests were completed.

Subthreshold SDS

Experiments were performed with GluN3A KO mice involving three consecutive 5 min physical interactions with a novel CD-1 mice, with a 15 min interval between each interaction[73].

Behavioral Assessments

Depression is a heterogeneous disease consisting of a set of symptoms as depressed mood, anhedonia, impaired concentration, feelings of worthlessness, hopelessness, suicidal thoughts, sleep and appetite disturbances, and psychomotor changes[7-10]. Thus, this study assessed the core symptom of depression, anhedonia,

using the SPT (sensory anhedonia) and the three-chamber SIT (social anhedonia). Locomotor activity related to psychomotor change symptoms was evaluated through the OFT, while helplessness behavior was measured using the TST and FST. Anxiety symptoms highly comorbid with depression were examined through the OFT and EPM.

All behavioral tests were conducted during the light cycle, with at least a 24h interval between different tests. 30min before each behavioral test, experimental mice were placed in a dimly lit testing room to acclimate to the environment. After each mouse completed the behavioral test, the apparatus was cleaned with 70% alcohol to eliminate residual mouse odors and traces. All test procedures were video-recorded.

SPT. During adaptation phase, mice were acclimatized for 48h by simultaneously giving one bottle of 1% sucrose solution and one bottle of pure water, and the bottle positions were switched after 24h of acclimatization in order to eliminate the position preference effect. During testing, the mice were deprived of water and food for 12h, followed by the placement of 1% sucrose solution and pure water for another 12h, and the amount of the two solutions consumed in testing phase was measured. The sucrose preference index was calculated as follows: Sucrose preference ratio (%) = Sucrose solution intake (g) / [Sucrose solution intake (g) + Pure water intake (g)] × 100%.

OFT. Mice were placed in the center of an open field arena (40×40×40 cm) to freely explore for 10min. The central square area (24×24 cm) was designated as the center zone. The total distance traveled in the open field, entries into the center zone,

and time spent in the center zone were automatically tracked using Anymaze software.

EPM. The EPM apparatus consists of a cross 50cm above the ground (single side arm 35cm long, 5cm wide, closed arm 15cm high). Mice were placed in the central area with their heads facing the open arm and allowed to freely explore for 5 min. The number of entries into the open arms and the time spent in the open arms were automatically tracked using Anymaze software. The percentage of time spent in the open arms (Open Arm Time Ratio) was calculated as follows: time spent in open arms (s) / [time spent in open arms (s) + time spent in closed arms (s)] × 100%.

SIT. The three-chamber test apparatus is an area (40 cm wide, 60 cm long, 20 cm high) divided into three equal areas by two transparent dividers with a shuttle channel at the bottom of the centre. A metal mesh cage is placed in the area on each side of the distal end. The testing process comprised two 10 min phases. During Phase 1 (adaptation phase), the test mouse is placed in the central area with the shuttle passage closed, allowing it to freely explore and familiarize itself with the environment. In Phase 2 (social test phase), an unfamiliar conspecific social mouse is placed in a metal cage on a random side area. The test mouse is then placed in the central area with the shuttle passage open, allowing free exploration of the three areas. Anymaze software automatically tracked the time the mouse spent in each area. The social interaction ratio was calculated as follows: Social interaction ratio (%) = Time spent in the social area (s) / [Time spent in the social area (s) + Time spent in the empty cage area (s)] × 100%.

TST. During testing, tape is attached to the tail tip of the experimental mouse, 1

cm from the end. A plastic tube is placed over the mouse's tail to prevent climbing. The mouse's tail is then secured to the top of the tail suspension apparatus, suspending the mouse approximately 25 cm above the ground for 6 min. The duration of immobility (s) during the 6 min video recording was recorded and analyzed.

FST. The experimental mouse is placed in a transparent cylindrical container (10 cm in diameter, 30 cm high) with water (25 cm deep, 25±1°C) to swim for 6 min. The duration of immobility (s) during the last 4 min of the 6 min video recording was quantified and analyzed.

Molecular biology test

This study employed Western blot and qRT-PCR to assess the mRNA and protein expression levels of GluN3A subunit in different brain regions of mice. Immunofluorescence staining, coupled with confocal imaging, was utilized for staining analysis of neurons in the CA1 region and their projection areas. Additionally, the spatial location of viral expression was confirmed by observing the fluorescence of the injected viruses in each experiment.

qRT-PCR. After rapidly decapitating the experimental mice, the brain was promptly dissected and placed in a freezing microtome. Specific brain region boundaries were delineated based on the mouse brain atlas, and target brain regions were extracted using a 1-mm-diameter tissue extraction needle [74], as shown in the fig1n. Total RNA was extracted from the tissue samples using TRIzol reagent (Cat# 15596018CN, Invitrogen, USA) following the manufacturer's instructions, and the concentration was analyzed using NanoDrop (Thermo Scientific, Massachusetts,

USA). Subsequently, 500 ng of RNA samples were reverse transcribed using the M-MLV Reverse Transcriptase (Cat# M1701, Promega, USA) following the reverse transcription kit instructions, with a two-step reaction condition: 70°C for 5 min, 37°C for 60 min, to generate cDNA. SYBR Green PCR Master Mix (Cat# CW2601M, Cowin Biotech, China) was used for fluorescence qPCR reactions. The real-time PCR instrument reaction steps were: a single cycle (95°C/10 min); 40 cycles (95°C/15 s; 60°C/1 min); a single cycle (95°C/15 s; 60°C/30 s; 95°C/15 s). Analysis was performed using the ΔΔC(t) method, with GAPDH as the reference gene for standardization. The primer sequences used were: Grin3A: forward: 5'-AGTACCTGAAGAATGATCCAGAGT-3', reverse: 5'-TCAGATATGTTAGAGGTCAACGG-3'; Gapdh: forward: 5'-ACCCACACTTCTC CATTTCC-3', reverse: 5'-TGGTTCCCAGGATAGGACTC-3'.

Western Blot. The target brain area tissue was homogenized in RIPA lysis buffer containing 1% PMSF (Cat# P0100, Solarbio, China). The collected protein supernatant was quantified using a BCA protein quantification kit (Cat# PC0020, Solarbio, China), and then protein samples were mixed with 4× protein loading buffer (Cat# P1015, Solarbio, China) for denaturation. The equal amounts of samples were loaded onto a 10% SDS-polyacrylamide gel (Cat# CW0022M, Cowin Biotech, China) for separation and then transferred to a 0.2 μm PVDF membrane (Cat# 03010040001, Millipore, Germany). The PVDF membrane was blocked in TBST solution containing 5% milk powder and then incubated overnight at 4°C with diluted primary antibodies (5% milk powder TBST): Grin3A (1:500; Cat# orb694249, Biorbyt, UK); Gapdh

(1:3000; Cat# 2118, Cell Signaling, USA). After washing with TBST, the membrane was incubated at room temperature for 2 h with secondary antibodies (5% milk powder TBST) containing horseradish peroxidase: Goat Anti-Rabbit IgG H&L (1:3000; Cat# ZB-2301, Zhongshan Golden Bridge, China). After washing again, the ECL luminescent liquid (Cat# P90719, Millipore, Germany) was added to the PVDF membrane, and the immunoblot signal was captured using an imaging system (FluorChem E, Protein Simple, California, USA).

Immunofluorescence Staining. 90 min after the completion of the FST or CNO injection, mice were intraperitoneally injected with pentobarbital (100 mg/kg) for anesthesia. Following anesthesia, mice were perfused with 30 ml of phosphate-buffered saline (PBS) through the heart, followed by 30 ml of 4% paraformaldehyde (PFA). The brain was removed, fixed in 4% PFA for 24 h at 4°C, and then transferred to PBS with 30% sucrose for dehydration. After the brain settled, 40 μm thick coronal hippocampal slices were obtained using a freezing microtome (CM3050S, Leica, Wetzlar, Germany) and stored at -80°C in an anti-freezing solution (50% PBS, 30% ethylene glycol, 20% glycerol). For immunofluorescence, the brain slices to be stained were washed with PBS, placed in PBST (0.1% TritonX-100, PBS) containing 5% goat serum at room temperature for 1.5 h, and then transferred to the primary antibody solution for overnight incubation at 4°C. The primary antibodies used were c-Fos (1:500; Cat# SYSY.226003, Synaptic Systems, Germany) and DYKDDDDK Tag (1:500; Cat#14793, Cell Signaling, USA). After washing with PBS, the slices were transferred to the secondary antibody solution at room temperature away from

light for 1.5 h. The secondary antibodies used were Goat Anti-Rabbit IgG H&L (Alexa Fluor® 488) (1:500; Cat# ab150077, Abcam, UK) and Goat anti-Rabbit IgG (H+L), Alexa Fluor™ 546 (1:500; Cat#A11010, Invitrogen, USA). After washing with PBS, the slices were incubated in PBS with DAPI (1:500; Cat# C0060, Solarbio, China) at room temperature away from light for 10 min. Following another PBS wash, the slices were mounted on glass slides using a mounting medium (Cat# ab104139, Abcam, UK).

Confocal Imaging and Analyses. Sliced brains or immunofluorescent stained brain slices were imaged using a high-speed confocal imaging system (SpinSR, Olympus, Tokyo, Japan) and a digital slice scanning and analysis system (DMI8, Leica, Wetzlar, Germany) under 10× and 20× objectives. Automated cell counting for c-Fos-positive neurons was performed using the ImageJ Fiji plugin (http://imagej.nih.gov/ij/). Two to four images were selected in each animal for statistical analysis of the brain regions.

In vivo manipulation

Viruses. AAV2/9-syn-m-Grin3A-3×flag-Null (titer 1.6×1012 vg/mL) and AAV2/9-syn-ZsGreen (titer 1.6×1012 vg/mL), AAV2/9-syn-hM3D(Gq)-mCherry (titer 1.2×1012 vg/mL), AAV2/9-syn-hM4D(Gi)-mCherry (titer 1.4×1012 vg/mL), and AAV2/9-syn-mCherry (titer 1.5×1012 vg/mL) were purchased from Hanbio Biotechnology, Shanghai, China. AAV2/PHP.eB-mCaMKIIα-GCaMP8s-WPRE-pA (titer 1.1×1013 vg/mL) was purchased from Taitool Bio, Shanghai, China. The viral vectors were aliquoted and stored at -80°C.

Stereotaxic surgery. Mice were anesthetized with isoflurane and secured in a stereotaxic apparatus (RWD Life Science, Shenzhen, China). After exposing the skull, the corresponding virus was slowly injected into the target location (AP: -2.90 mm; ML ± 3.30 mm; DV: -2.90 mm) using a Stoelting pump (QSI storage pump, Stoelting, Wisconsin, USA) attached to a Hamilton syringe. After injection, the syringe was left in place for 10 min before slow withdrawal. The mice were allowed to recover for 14 days before behavioral testing.

Regulation of GluN3A subunit experiments. 0.15 μL (unilateral) of AAV2/9-syn-m-Grin3A-3×flag-Null or AAV2/9-syn-ZsGreen was bilaterally injected into CA1i at a rate of 0.05 μL/min.

Chemogenetic experiments. 0.15 μL (unilateral) of AAV2/9-syn-hM3D(Gq)-mCherry or AAV2/9-syn-hM4D(Gi)-mCherry (or AAV2/9-syn-mCherry) was injected into each hemisphere of CA1i at a rate of 0.05 μL/min. 14 days later, Clozapine N-oxide (CNO, Cat# HY-17366, MCE, USA) was dissolved in dimethyl sulfoxide (DMSO, Cat# D8418, Sigma, Germany) to create a 100 mg/mL stock solution. Before injection, further dilution was made with 0.9% saline to achieve a CNO injection quality of 0.2 mg/kg (injection volume: 10 mL/kg) for chemogenetic activation experiments and 2 mg/kg for chemogenetic inhibition experiments. CNO was intraperitoneally injected 30 min before behavioral testing.

Fiber photometry experiments. AAV2/PHP.eB-mCaMKIIα-GCaMP8s-WPRE-pA was diluted 1:4 in cerebrospinal fluid. 0.2 μL (unilateral) of the viral diluted solution was injected into the bilateral CA1i at a rate of 0.05 μL/min. Then, a ceramic

optical fiber (200 μm in diameter, 3 mm length, 0.37 NA, Inper Technology Co., Ltd., Hangzhou, China) was implanted above the CA1i region (AP: -2.90 mm; ML ±3.30 mm; DV: -2.85 mm). The fiber was secured to the skull with dental cement. 14 days later, power levels of 470 nm excitation light and 410 nm excitation light in the Inper Signal fiber photometry system (Inper Technology Co., Ltd., Hangzhou, China) were measured using a photometer and adjusted to 25 μW and 10-15 μW, respectively. Prior to the TST, the bundled fiber was connected to the optical fiber implant in the mouse's head for a two-min adaptation. The Inper Signal system recorded Ca2+ activity in the CA1i region of mice suspended and during tail suspension tests, synchronizing with a camera to record the behavioral state. Inper Plot software was used to analyze and statistically process the fluorescence change data (F) during hanging and struggling events, calculating the relative fluorescence change ΔF/F0 (ΔF/F0 = (F-F0)/F0). Mice with fiber implantation positions confirming the expected target were included in data analysis.

Drug delivery experiments. After injecting chemogenetic viruses into bilateral CA1i, 22-gauge single-guide cannulas (RWD Life Science, Shenzhen, China) were bilaterally implanted 0.5 mm above the target positions (AP: -2.90 mm; ML: ±3.30 mm; DV: -2.40 mm). The cannulas were fixed on the skull surface with dental cement. 14 days later, 10 mg/mL D-serine was prepared in CSF. 30 min before the behavioral test, mice were anesthetized with isoflurane, and an injection inner tube exceeding the cannula target position by 0.5 mm was inserted into the mouse's head cannula. Subsequently, using a dual-channel microinjection pump (RWD Life Science,

Shenzhen, China), 0.5 μL (unilateral) of D-serine or CSF was injected into the bilateral CA1i region at a rate of 0.2 μL/min. After completion, the inner tube was left in place for 5 min before slow withdrawal.

Statistical Analysis

All data are presented as mean ± standard error of the mean (M±SEM) and analyzed using GraphPad Prism 9.0 software. Normality distribution was assessed using the Anderson-Darling test. Differences between two groups were evaluated using unpaired Student's t-test, and when variances were unequal, Welch's correction was applied. Analysis of variance with one or two factors was used for comparisons among three groups or more, followed by False discovery rate (FDR): Benjamini-Krieger-Yekutieli correction for multiple comparisons. A p-value < 0.05 was considered statistically significant.

Acknowledgements

We are grateful to the lab of Tifei Yuan (Shanghai Mental health center, Shanghai, China) for providing the GluN3A KO mice. We greatly appreciate the excellent work of the technical support staff at the Institutional Center for Shared Technologies and Facilities of Institute of Psychology, Chinese Academy of Sciences. This work was supported by the National Natural Science Foundation of China [Grant No. 82071517, U21A20364, 31900731], National Key R&D Program of China [Grant No. 2017YFE0126500], and the Scientific Foundation of Institute of Psychology, Chinese Academy of Sciences (No. E2CX4115CX).

Author contributions

Methodology, data curation and investigation, writing-original draft & editing: WZ; Research conceptualization, project administration, funding acquisition and editing: JW; Research conceptualization, resources, project administration, funding acquisition, supervision and writing-review & editing: WW; Methodology: JD, LZ, MZ, and HY participated.

Conflict of Interest

The authors declare no competing interests.

Additional information

Supplementary information has been provided to the website.

References

1. Collaborators GBDMD. Global, regional, and national burden of 12 mental disorders in 204 countries and territories, 1990-2019: a systematic analysis for the Global Burden of Disease Study 2019. *Lancet Psychiatry* 2022; **9**(2)**:** 137-150.

2. Bai R, Dong W, Peng Q, Bai Z. Trends in depression incidence in China, 1990-2019. *J Affect Disord* 2022; **296:** 291-297.

3. Sahli ZT, Banerjee P, Tarazi FI. The Preclinical and Clinical Effects of Vilazodone for the Treatment of Major Depressive Disorder. *Expert Opin Drug Discov* 2016; **11**(5)**:** 515-523.

4. Kostev K, Ehlken B, Rex J, Engelhard J, Altmann V, Heilmaier C. Which Adverse Effects Influence the Dropout Rate in Selective Serotonin Reuptake Inhibitor (Ssri) Treatment? *Value Health* 2014; **17**(7)**:** A460-A460.

5. Yuet WC, Derasari D, Sivoravong J, Mason D, Jann M. Selective Serotonin Reuptake Inhibitor Use and Risk of Gastrointestinal and Intracranial Bleeding. *J Am Osteopath Assoc* 2019; **119**(2)**:** 102-111.

6. Friedman RA. Antidepressants' black-box warning--10 years later. *N Engl J Med* 2014; **371**(18)**:** 1666-1668.

7. Pizzagalli DA, Roberts AC. Prefrontal cortex and depression. *Neuropsychopharmacology* 2022; **47**(1)**:** 225-246.

8. Lynall ME, McIntosh AM. The Heterogeneity of Depression. *Am J Psychiatry* 2023; **180**(10)**:** 703-704.

9. Lynch CJ, Gunning FM, Liston C. Causes and Consequences of Diagnostic Heterogeneity in Depression: Paths to Discovering Novel Biological Depression Subtypes. *Biol Psychiatry* 2020; **88**(1)**:** 83-94.

10. Winter S. Gender trouble: The World Health Organization, the International Statistical Classification of Diseases and Related Health Problems (ICD)-11 and the trans kids. *Sex Health* 2017; **14**(5)**:** 423-430.

11. Xu H, Wang J, Jing H, Ellenbroek B, Shao F, Wang W. mPFC GABAergic transmission mediated the role of BDNF signaling in cognitive impairment but not anxiety induced by adolescent social stress. *Neuropharmacology* 2021; **184:** 108412.

12. Preti A. Animal model and neurobiology of suicide. *Prog Neuropsychopharmacol Biol Psychiatry* 2011; **35**(4)**:** 818-830.

13. Roy B, Dwivedi Y. Modeling endophenotypes of suicidal behavior in animals. *Neurosci Biobehav Rev* 2021; **128:** 819-827.

14. Lv S, Yao K, Zhang Y, Zhu S. NMDA receptors as therapeutic targets for depression treatment: Evidence from clinical to basic research. *Neuropharmacology* 2023; **225:** 109378.

15. Amidfar M, Woelfer M, Reus GZ, Quevedo J, Walter M, Kim YK. The role of NMDA receptor in neurobiology and treatment of major depressive disorder: Evidence from translational research. *Prog Neuropsychopharmacol Biol Psychiatry* 2019; **94:** 109668.

16. Duman RS, Sanacora G, Krystal JH. Altered Connectivity in Depression: GABA and Glutamate Neurotransmitter Deficits and Reversal by Novel Treatments. *Neuron* 2019; **102**(1)**:** 75-90.

17. Shi X, Zhang Q, Li J, Liu X, Zhang Y, Huang M *et al.* Disrupting phosphorylation of Tyr-1070 at GluN2B selectively produces resilience to depression-like behaviors. *Cell Rep* 2021; **36**(8)**:** 109612.

18. Skolnick P, Layer RT, Popik P, Nowak G, Paul IA, Trullas R. Adaptation of N-methyl-D-aspartate (NMDA) receptors following antidepressant treatment: implications for the pharmacotherapy of depression. *Pharmacopsychiatry* 1996; **29**(1)**:** 23-26.

19. Skolnick P. Antidepressants for the new millennium. *Eur J Pharmacol* 1999; **375**(1-3)**:** 31-40.

20. Nowak G, Li Y, Paul IA. Adaptation of cortical but not hippocampal NMDA receptors after chronic citalopram treatment. *Eur J Pharmacol* 1996; **295**(1)**:** 75-85.

21. Ma S, Chen M, Jiang Y, Xiang X, Wang S, Wu Z *et al.* Sustained antidepressant effect of ketamine through NMDAR trapping in the LHb. *Nature* 2023; **622**(7984)**:** 802-809.

22. Su T, Lu Y, Fu C, Geng Y, Chen Y. GluN2A mediates ketamine-induced rapid antidepressant-like responses. *Nat Neurosci* 2023; **26**(10)**:** 1751-1761.

23. Rozet I. Ketamine in depression and electroconvulsive therapy. *Curr Opin Anaesthesiol* 2021; **34**(5)**:** 556-562.

24. Treccani G, Ardalan M, Chen F, Musazzi L, Popoli M, Wegener G *et al.* S-Ketamine Reverses Hippocampal Dendritic Spine Deficits in Flinders Sensitive Line Rats Within 1 h of Administration. *Mol Neurobiol* 2019; **56**(11)**:** 7368-7379.

25. Aleksandrova LR, Wang YT, Phillips AG. Ketamine and its metabolite, (2R,6R)-HNK, restore hippocampal LTP and long-term spatial memory in the Wistar-Kyoto rat model of depression. *Mol Brain* 2020; **13**(1)**:** 92.

26. Liu B, Liu J, Wang M, Zhang Y, Li L. From Serotonin to Neuroplasticity: Evolvement of Theories for Major Depressive Disorder. *Front Cell Neurosci* 2017; **11:** 305.

27. Pachernegg S, Strutz-Seebohm N, Hollmann M. GluN3 subunit-containing NMDA receptors: not just one-trick ponies. *Trends Neurosci* 2012; **35**(4)**:** 240-249.

28. Perez-Otano I, Larsen RS, Wesseling JF. Emerging roles of GluN3-containing NMDA receptors in the CNS. *Nat Rev Neurosci* 2016; **17**(10)**:** 623-635.

29. Zhu S, Paoletti P. Allosteric modulators of NMDA receptors: multiple sites and mechanisms. *Curr Opin Pharmacol* 2015; **20:** 14-23.

30. Yan J, Bengtson CP, Buchthal B, Hagenston AM, Bading H. Coupling of NMDA receptors and TRPM4 guides discovery of unconventional neuroprotectants. *Science* 2020; **370**(6513).

31. Beesley S, Sullenberger T, Kumar SS. The GluN3 subunit regulates ion selectivity within native N-methyl-d-aspartate receptors. *IBRO Rep* 2020; **9:** 147-156.

32. Bossi S, Dhanasobhon D, Ellis-Davies GCR, Frontera J, de Brito Van Velze M, Lourenco J *et al.* GluN3A excitatory glycine receptors control adult cortical and amygdalar circuits. *Neuron* 2022; **110**(15)**:** 2438-2454 e2438.

33. Bossi S, Pizzamiglio L, Paoletti P. Excitatory GluN1/GluN3A glycine receptors (eGlyRs) in brain signaling. *Trends Neurosci* 2023; **46**(8)**:** 667-681.

34. Conde-Dusman MJ, Dey PN, Elia-Zudaire O, Rabaneda LG, Garcia-Lira C, Grand T *et al.* Control of protein synthesis and memory by GluN3A-NMDA receptors through inhibition of GIT1/mTORC1 assembly. *Elife* 2021; **10**.

35. Crawley O, Conde-Dusman MJ, Perez-Otano I. GluN3A NMDA receptor subunits: more enigmatic than ever? *J Physiol* 2022; **600**(2)**:** 261-276.

36. Zhong W, Wu A, Berglund K, Gu X, Jiang MQ, Talati J *et al.* Pathogenesis of sporadic Alzheimer's disease by deficiency of NMDA receptor subunit GluN3A. *Alzheimers Dement* 2022; **18**(2)**:** 222-239.

37. Henson MA, Roberts AC, Perez-Otano I, Philpot BD. Influence of the NR3A subunit on NMDA receptor functions. *Prog Neurobiol* 2010; **91**(1)**:** 23-37.

38. Mohamad O, Song M, Wei L, Yu SP. Regulatory roles of the NMDA receptor GluN3A subunit in locomotion, pain perception and cognitive functions in adult mice. *J Physiol* 2013; **591**(1)**:** 149-168.

39. Roberts AC, Diez-Garcia J, Rodriguiz RM, Lopez IP, Lujan R, Martinez-Turrillas R *et al.* Downregulation of NR3A-containing NMDARs is required for synapse maturation and memory consolidation. *Neuron* 2009; **63**(3)**:** 342-356.

40. Murillo A, Navarro AI, Puelles E, Zhang Y, Petros TJ, Perez-Otano I. Temporal Dynamics and Neuronal Specificity of Grin3a Expression in the Mouse Forebrain. *Cereb Cortex* 2021; **31**(4)**:** 1914-1926.

41. Henson MA, Larsen RS, Lawson SN, Perez-Otano I, Nakanishi N, Lipton SA *et al.* Genetic deletion of NR3A accelerates glutamatergic synapse maturation. *PLoS One* 2012; **7**(8)**:** e42327.

42. Otsu Y, Darcq E, Pietrajtis K, Matyas F, Schwartz E, Bessaih T *et al.* Control of aversion by glycine-gated GluN1/GluN3A NMDA receptors in the adult medial habenula. *Science* 2019; **366**(6462)**:** 250-254.

43. Zhang M, Kong X, Chen J, Liu W, Liu C, Dou X *et al.* Dysfunction of GluN3A subunit is involved in depression-like behaviors through synaptic deficits. *J Affect Disord* 2023; **332:** 72-82.

44. Rao JS, Harry GJ, Rapoport SI, Kim HW. Increased excitotoxicity and neuroinflammatory markers in postmortem frontal cortex from bipolar disorder patients. *Mol Psychiatry* 2010; **15**(4)**:** 384-392.

45. Roddy DW, Farrell C, Doolin K, Roman E, Tozzi L, Frodl T *et al.* The Hippocampus in Depression: More Than the Sum of Its Parts? Advanced Hippocampal Substructure Segmentation in Depression. *Biol Psychiatry* 2019; **85**(6)**:** 487-497.

46. Schloesser RJ, Jimenez DV, Hardy NF, Paredes D, Catlow BJ, Manji HK *et al.* Atrophy of pyramidal neurons and increased stress-induced glutamate levels in CA3 following chronic suppression of adult neurogenesis. *Brain Struct Funct* 2014; **219**(3)**:** 1139-1148.

47. Anacker C, Luna VM, Stevens GS, Millette A, Shores R, Jimenez JC *et al.* Hippocampal neurogenesis confers stress resilience by inhibiting the ventral dentate gyrus. *Nature* 2018; **559**(7712)**:** 98-102.

48. Kaiser RH, Andrews-Hanna JR, Wager TD, Pizzagalli DA. Large-Scale Network Dysfunction in Major Depressive Disorder: A Meta-analysis of Resting-State Functional Connectivity. *JAMA Psychiatry* 2015; **72**(6)**:** 603-611.

49. Duman RS, Aghajanian GK, Sanacora G, Krystal JH. Synaptic plasticity and depression: new insights from stress and rapid-acting antidepressants. *Nat Med* 2016; **22**(3)**:** 238-249.

50. Li Y, Fan C, Wang C, Wang L, Yi Y, Mao X *et al.* Stress-induced reduction of Na(+)/H(+) exchanger isoform 1 promotes maladaptation of neuroplasticity and exacerbates depressive behaviors. *Sci Adv* 2022; **8**(45)**:** eadd7063.

51. Schultz C, Engelhardt M. Anatomy of the hippocampal formation. *Front Neurol Neurosci* 2014; **34:** 6-17.

52. Fanselow MS, Dong HW. Are the dorsal and ventral hippocampus functionally distinct structures? *Neuron* 2010; **65**(1)**:** 7-19.

53. Bienkowski MS, Bowman I, Song MY, Gou L, Ard T, Cotter K *et al.* Integration of gene expression and brain-wide connectivity reveals the multiscale organization of mouse hippocampal networks. *Nat Neurosci* 2018; **21**(11)**:** 1628-1643.

54. Okuyama T, Kitamura T, Roy DS, Itohara S, Tonegawa S. Ventral CA1 neurons store social memory. *Science* 2016; **353**(6307)**:** 1536-1541.

55. Grand T, Abi Gerges S, David M, Diana MA, Paoletti P. Unmasking GluN1/GluN3A excitatory glycine NMDA receptors. *Nat Commun* 2018; **9**(1)**:** 4769.

56. Zhu Z, Yi F, Epplin MP, Liu D, Summer SL, Mizu R *et al.* Negative allosteric modulation of GluN1/GluN3 NMDA receptors. *Neuropharmacology* 2020; **176:** 108117.

57. Machado-Vieira R, Henter ID, Zarate CA, Jr. New targets for rapid antidepressant action. *Prog Neurobiol* 2017; **152:** 21-37.

58. Park M, Niciu MJ, Zarate CA, Jr. Novel Glutamatergic Treatments for Severe Mood Disorders. *Curr Behav Neurosci Rep* 2015; **2**(4)**:** 198-208.

59. Preskorn S, Macaluso M, Mehra DO, Zammit G, Moskal JR, Burch RM *et al.* Randomized proof of concept trial of GLYX-13, an N-methyl-D-aspartate receptor glycine site partial agonist, in major depressive disorder nonresponsive to a previous antidepressant agent. *J Psychiatr Pract* 2015; **21**(2)**:** 140-149.

60. Ragguett RM, Rong C, Kratiuk K, McIntyre RS. Rapastinel - an investigational NMDA-R modulator for major depressive disorder: evidence to date. *Expert Opin Investig Drugs* 2019; **28**(2)**:** 113-119.

61. Wang J, Zhang K, Chen X, Liu X, Teng H, Zhao M *et al.* Epigenetic Activation of ASCT2 in the Hippocampus Contributes to Depression-Like Behavior by Regulating D-Serine in Mice. *Front Mol Neurosci* 2017; **10:** 139.

62. MacKay MB, Kravtsenyuk M, Thomas R, Mitchell ND, Dursun SM, Baker GB. D-Serine: Potential Therapeutic Agent and/or Biomarker in Schizophrenia and Depression? *Front Psychiatry* 2019; **10:** 25.

63. Otte DM, Barcena de Arellano ML, Bilkei-Gorzo A, Albayram O, Imbeault S, Jeung H *et al.* Effects of Chronic D-Serine Elevation on Animal Models of Depression and Anxiety-Related Behavior. *PLoS One* 2013; **8**(6)**:** e67131.

64. Yao Y, Mayer ML. Characterization of a soluble ligand binding domain of the NMDA receptor regulatory subunit NR3A. *J Neurosci* 2006; **26**(17)**:** 4559-4566.

65. Zhang J, Liu X, Fang L. Combined effects of depression and anxiety on suicide: A case-control psychological autopsy study in rural China. *Psychiatry Res* 2019; **271:** 370-373.

66. Berardelli I, Sarubbi S, Rogante E, Hawkins M, Cocco G, Erbuto D *et al.* The Role of Demoralization and Hopelessness in Suicide Risk in Schizophrenia: A Review of the Literature. *Medicina (Kaunas)* 2019; **55**(5).

67. Lu CY, Zhang F, Lakoma MD, Madden JM, Rusinak D, Penfold RB *et al.* Changes in antidepressant use by young people and suicidal behavior after FDA warnings and media coverage: quasi-experimental study. *BMJ* 2014; **348:** g3596.

68. Domany Y, Shelton RC, McCullumsmith CB. Ketamine for acute suicidal ideation. An emergency department intervention: A randomized, double-blind, placebo-controlled, proof-of-concept trial. *Depress Anxiety* 2020; **37**(3)**:** 224-233.

69. Lee JH, Wei L, Deveau TC, Gu X, Yu SP. Expression of the NMDA receptor subunit GluN3A (NR3A) in the olfactory system and its regulatory role on olfaction in the adult mouse. *Brain Struct Funct* 2016; **221**(6)**:** 3259-3273.

70. Gonzalez-Gonzalez IM, Gray JA, Ferreira J, Conde-Dusman MJ, Bouchet D, Perez-Otano I *et al.* GluN3A subunit tunes NMDA receptor synaptic trafficking and content during postnatal brain development. *Cell Rep* 2023; **42**(5)**:** 112477.

71. Malkesman O, Austin DR, Tragon T, Wang G, Rompala G, Hamidi AB *et al.* Acute D-serine treatment produces antidepressant-like effects in rodents. *Int J Neuropsychopharmacol* 2012; **15**(8)**:** 1135-1148.

72. Poleszak E, Szewczyk B, Wlaz A, Fidecka S, Wlaz P, Pilc A *et al.* D-serine, a selective glycine/N-methyl-D-aspartate receptor agonist, antagonizes the antidepressant-like effects of magnesium and zinc in mice. *Pharmacol Rep* 2008; **60**(6)**:** 996-1000.

73. Menard C, Pfau ML, Hodes GE, Kana V, Wang VX, Bouchard S *et al.* Social stress induces neurovascular pathology promoting depression. *Nat Neurosci* 2017; **20**(12)**:** 1752-1760.

74. Franklin KBJ, Paxinos G. *Paxinos and Franklin's The mouse brain in stereotaxic coordinates*. Fourth edition. edn. Academic Press, an imprint of Elsevier: Amsterdam, 2013, 1 volume (unpaged)pp.

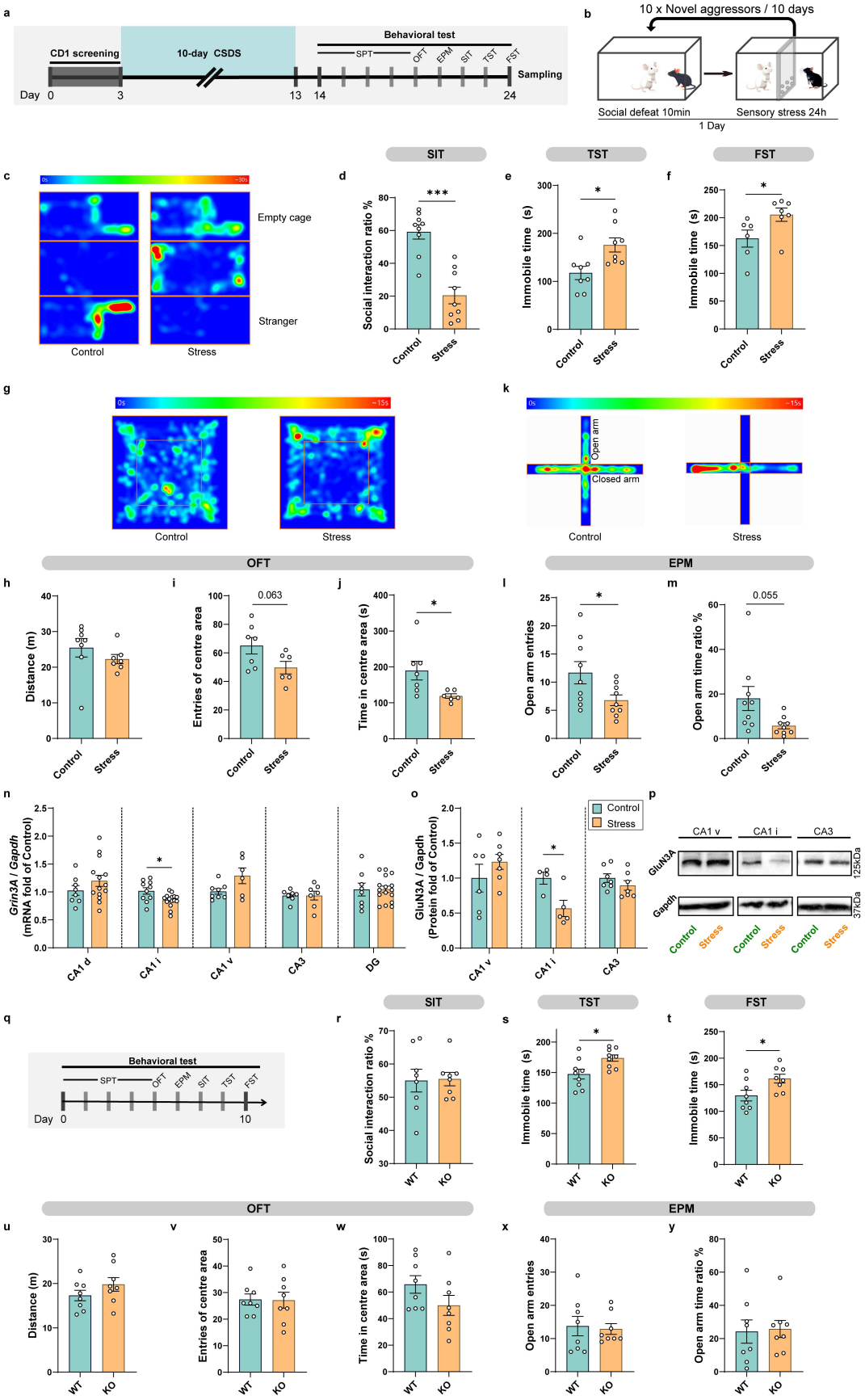

Figure1. CSDS and GluN3A KO induced depression-related behaviors in mice and

reduced GluN3A expression in the CA1i region of CSDS mice.

a Experimental scheme of CSDS modeling and behavioral tests. **b** Schematic of CSDS. **c** Example trajectory heatmap of SIT in control mice (left) and stress mice (right). **d** Social interaction ratio of SIT (n = 9 mice per group). **e** Immobility time in the TST (n = 8 mice per group). **f** Immobility time in the FST (n = 6-7 mice per group). **g** Example trajectory heatmap of OFT in control mice (left) and stress mice (right). **h** The total distance traveled in OFT (n = 7-8 mice per group). **i** The number of entries to centre area of OFT (n = 6-7 mice per group). **j** The time in the centre area of OFT (n = 6-7 mice per group). **k** Example trajectory heatmap of EPM in control mice (left) and stress mice (right). **l** The number of entries to open arms of EPM (n = 9 mice per group). **m** Percentage of time spent in the open arms of EPM (n = 9 mice per group). **n** Quantitative data of *Grin3A* mRNA in target brain area from control and stress mice (n = 6-16 mice per group). **o** Quantitative data of GluN3A protein in target brain area from control and stress mice (n = 4-7 mice per group). **p** Representative western blots for dissected target brain area. **q** Experimental scheme of behavioral studies. **r** Social interaction ratio of SIT (n = 8 mice per group). **s** Immobility time in the TST (n = 9 mice per group). **t** Immobility time in the FST (n = 8 mice per group). **u** The total distance traveled in OFT (n = 8 mice per group). **v** The entries of centre area in OFT (n = 8 mice per group). **w** The time in the centre area of OFT (n = 8 mice per group). **x** The number of entries to open arms of EPM (n = 8 mice per group). **y** Percentage of time spent in the open arms of EPM (n = 8 mice per group). * $P < 0.05$, *** $P < 0.001$.

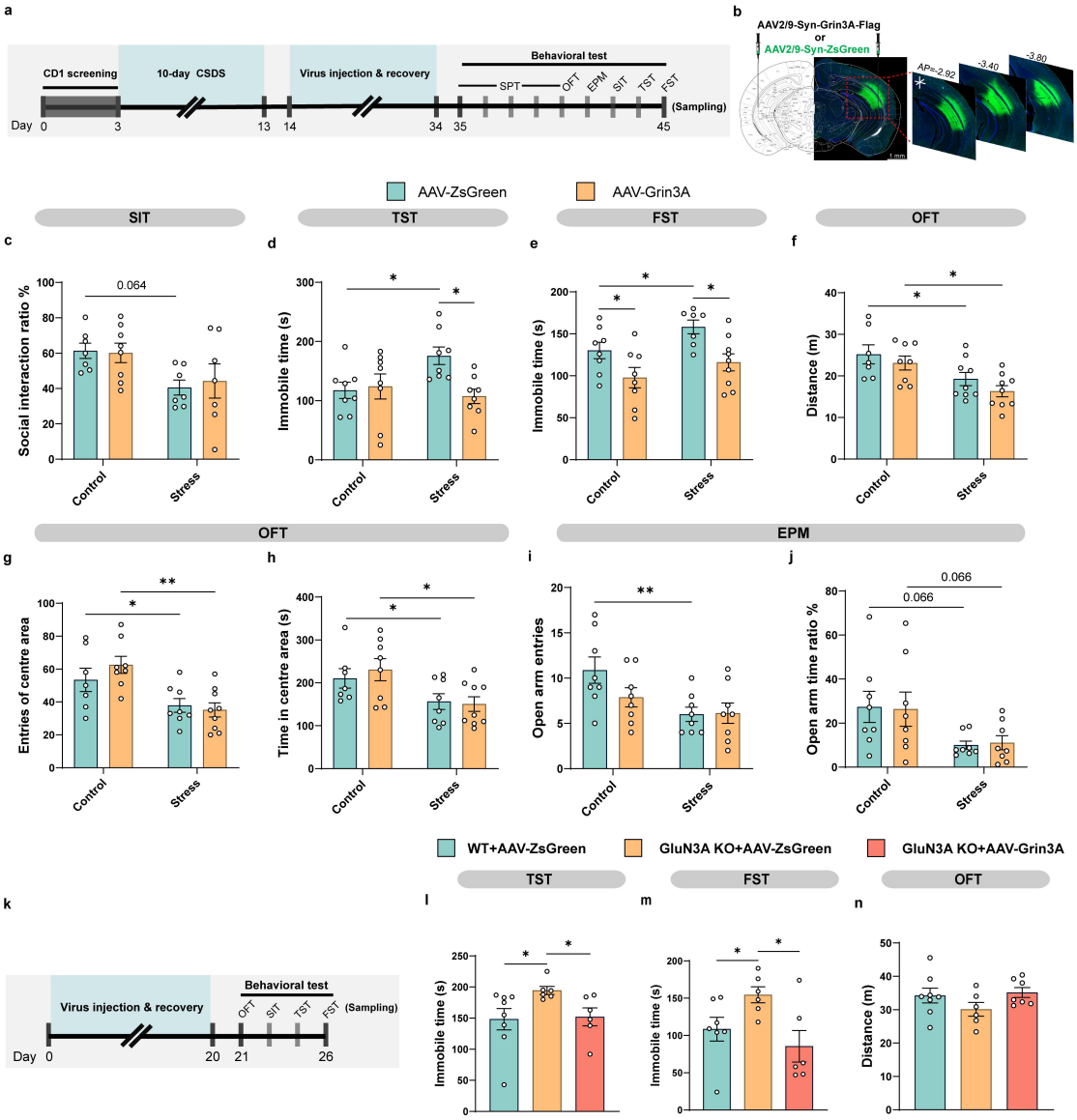

Figure2. Overexpression of GluN3A in CA1i reversed the helplessness behavior in CSDS mice and GluN3A KO mice.

a Experimental scheme of CSDS modeling, virus injection, and behavior tests. **b** Schematic target locations and immunofluorescence images of ZsGreen or flag expression of Virus in the CA1i. Scale bar, 1 mm. **c** Social interaction ratio of SIT (*n* = 7-8 mice per group). **d** Immobility time in the TST (*n* = 8 mice per group). **e** Immobility time in the FST (*n* = 7-9 mice per group). **f** The total distance traveled in OFT (*n* = 7-9 mice per group). **g** The number of entries to centre area of OFT (*n* = 7-9 mice per group). **h** The time in the centre area of OFT (*n* = 7-9 mice per group). **i** The

number of entries to open arms of EPM (n = 8 mice per group). **j** Percentage of time spent in the open arms of EPM (n = 8 mice per group). **k** Experimental scheme of virus injection and behavior tests. **l** Immobility time in the TST (n = 6-8 mice per group). **m** Immobility time in the FST (n = 6-7 mice per group). **n** The total distance traveled in OFT (n = 6-8 mice per group). * $P < 0.05$, ** $P < 0.01$.

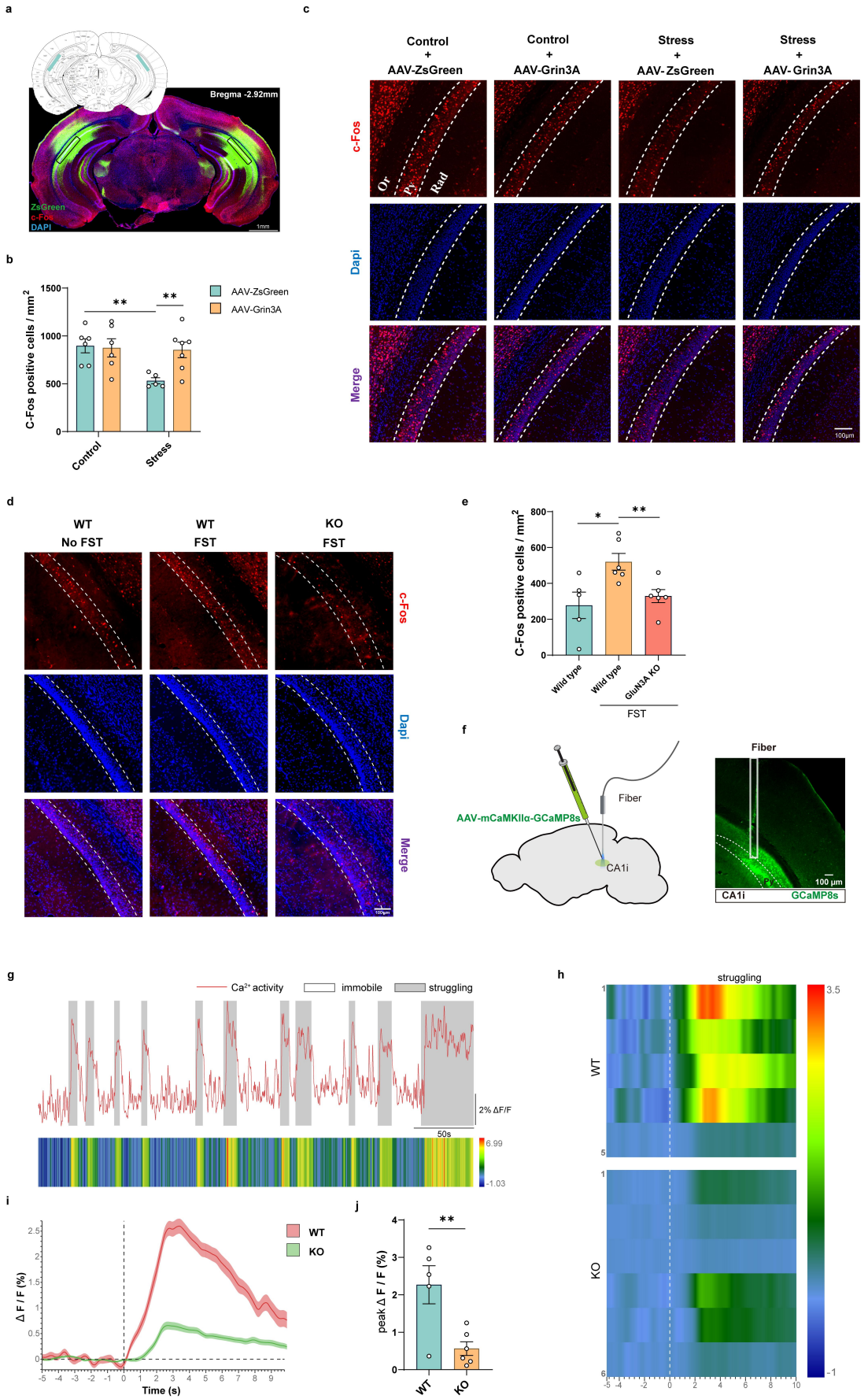

Figure3. Activity of CA1i pyramidal neurons mediated the regulation of GluN3A in

helplessness behavior.

a Statistical region of c-Fos-positive cells in CA1i (ZsGreen: green, c-Fos: red, Dapi: blue). Scale bar, 1 mm. **b** Quantification of c-Fos-positive cells in CA1i pyramidal layer neurons of each group of mice. (n = 5-7 mice per group, 4 slices for each mouse). **c-d** Representative images of c-Fos-positive cells in the CA1i of each group of mice (c-Fos: red, Dapi: blue). Scale bar, 100 μm. **e** Quantification of c-Fos-positive cells in CA1i pyramidal layer neurons of each group of mice. (n = 5-6 mice per group, 4 slices for each mouse). **f** Schematic illustrating fiber placement and representative images of GCaMP8s expression. Scale bar, 100 μm. **g** Top, Example fluorescence trace of the GCaMP signal during TST. Gray shaded area indicates struggling behavior; white area indicates immobile behavior. Bottom, heatmap of fluorescence intensity. **h** Representative heatmaps of GCaMP8s transient ΔF/F event locked to struggling. Each row plots one mice, and a total of 11 mice are illustrated. **i** Dynamics of GCamp8s signaling in mice 5 seconds before and 10 seconds after struggling in the TST (mean ΔF/F ± s.e.m.). **j** Changes in average ΔF/F of WT and KO mice during the struggle (n = 5-6 mice per group). * $P < 0.05$, ** $P < 0.01$.

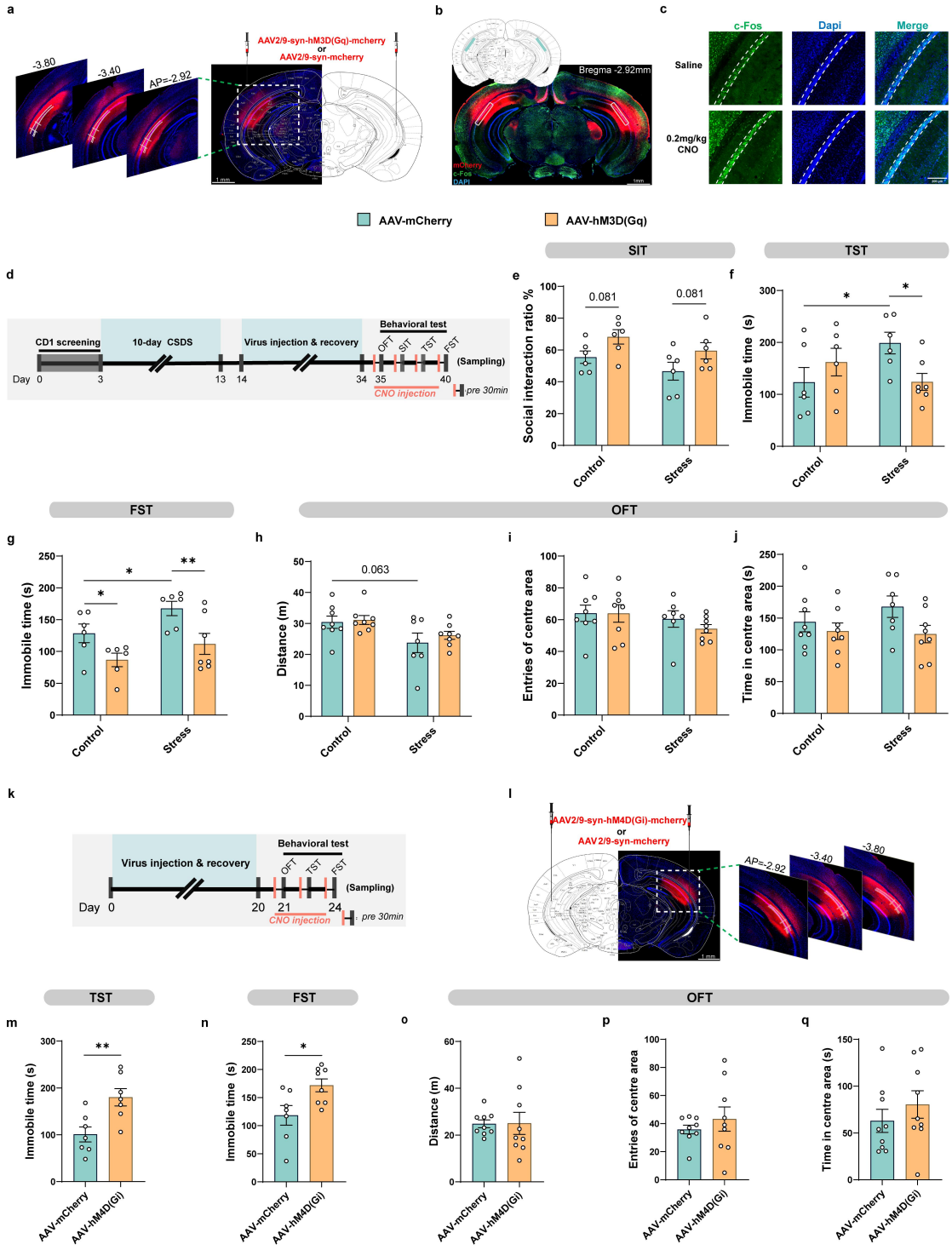

Figure4. Bidirectional chemogenetic modulation of CA1i pyramidal neurons directly mimicked or reversed the CSDS-induced helplessness behavior.

a Schematic target locations and immunofluorescence images of hM3D(Gq)-mCherry or mCherry expression of Virus in the CA1i. Scale bar, 1 mm. **b** Statistical regions of c-Fos-positive cells in

CA1i (mCherry: red, c-Fos: green, Dapi: blue). Scale bar, 1 mm. **c** Representative images of c-Fos-positive cells in the CA1i of the saline and 0.2 mg/kg CNO treatment mice (c-Fos: green, Dapi: blue). Scale bar, 200 μm. **d** Experimental scheme of CSDS modeling, virus injection, and behavior tests without or with chemogenetic activation. **e** Social interaction ratio of SIT (n = 6 mice per group). **f** Immobility time in the TST (n = 6-7 mice per group). **g** Immobility time in the FST (n = 6-7 mice per group). **h** The total distance traveled in OFT (n = 7-8 mice per group). **i** The number of entries to centre area of OFT (n = 7-8 mice per group). **j** The time in the centre area of OFT (n = 7-8 mice per group). **k** Experimental scheme of virus injection, and behavior tests without or with chemogenetic inactivation. **l** Schematic target locations and immunofluorescence images of hM4D(Gi)-mCherry or mCherry expression of Virus in the CA1i. Scale bar, 1 mm. **m** Immobility time in the TST (n = 7 mice per group). **n** Immobility time in the FST (n = 7-8 mice per group). **o** The total distance traveled in OFT (n = 9 mice per group). **p** The number of entries to centre area of OFT (n = 9 mice per group). **q** The time in the centre area of OFT (n = 9 mice per group). * $P < 0.05$, ** $P < 0.01$.

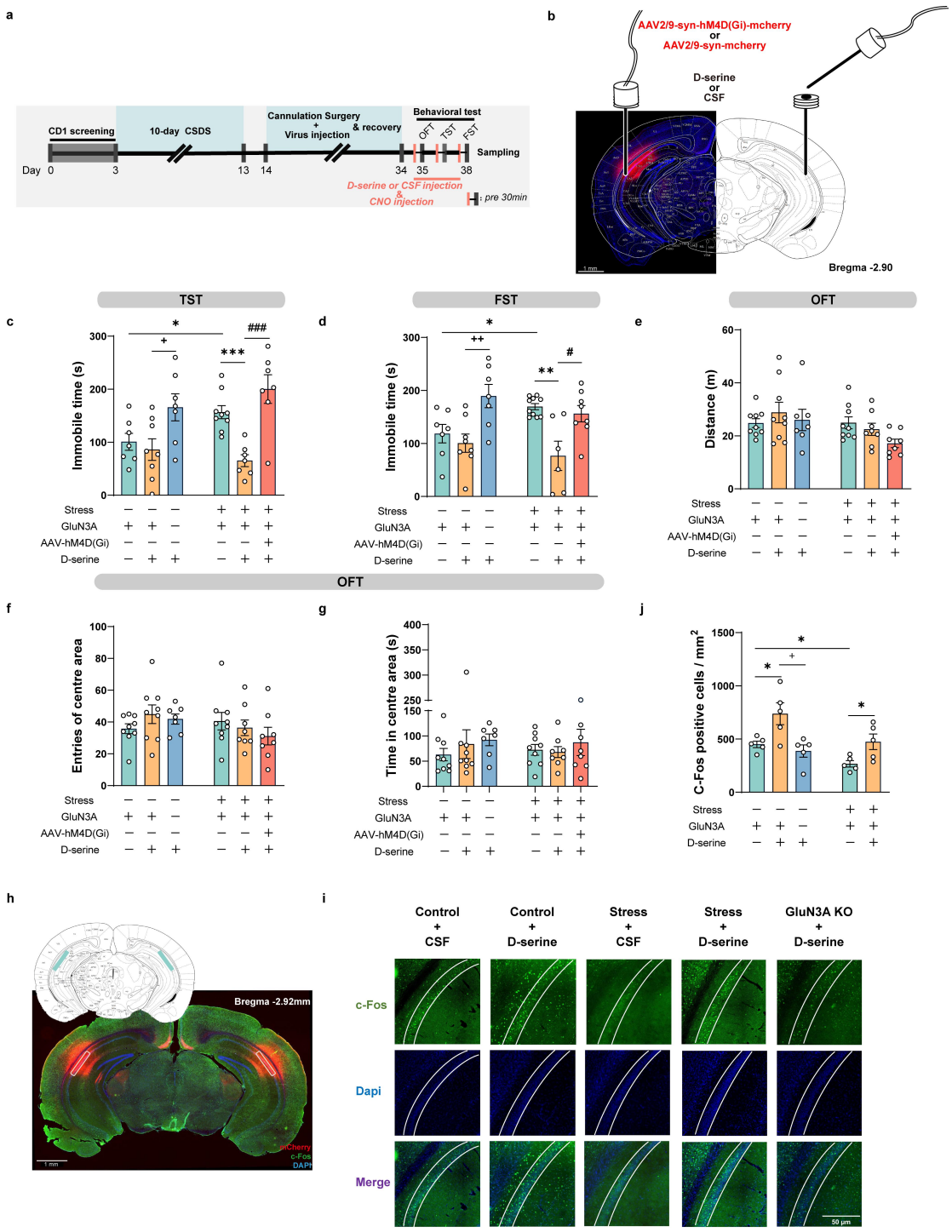

Figure5. Potentiation of GluN3A-mediated pyramidal neuronal activity in CA1i was necessary for the rapid antidepressant effects of D-serine

a Experimental scheme of CSDS modeling, virus injection, cannula implantation, and behavior tests without or with D-serine delivery. **b** Schematic target locations injection of D-serine (CSF) and Virus in the CA1i. Scale bar, 1 mm. **c** Immobility time in the TST (*n* = 7-9 mice per group). **d**

Immobility time in the FST (n = 6-10 mice per group). **e** The total distance traveled in OFT (n = 7-9 mice per group). **f** The number of entries to centre area of OFT (n = 7-9 mice per group). **g** The time in the centre area of OFT (n = 7-9 mice per group). **h** Statistical regions of c-Fos-positive cells in CA1i (mCherry: red, c-Fos: green, Dapi: blue). Scale bar, 1 mm. **i** Representative images of c-Fos-positive cells in the CA1i of each group of mice (c-Fos: green, Dapi: blue). Scale bar, 50 μm. **j** Quantification of c-Fos-positive cells in CA1i pyramidal layer neurons of each group of mice. (per mm, n = 5 mice per group, 4 slices for each mouse). * $P < 0.05$, ** $P < 0.01$, *** $P < 0.001$; $^{+}$ $P < 0.05$, $^{++}$ $P < 0.01$; $^{\#}$ $P < 0.05$, $^{\#\#\#}P < 0.001$.